IET Power Electronics

Research Article

IET Journals
The Institution of Engineering and Technology

Enhanced direct torque control and predictive torque control strategies of an open-End winding induction motor drive to eliminate common-mode voltage and weighting factors

ISSN 1755-4535
Received on 22nd June 2018
Revised 21st February 2019
Accepted on 1st April 2019
E-First on 25th June 2019
doi: 10.1049/iet-pel.2018.5599
www.ietdl.org

Kunisetti V Praveen Kumar[1] ✉, *Thippiripati Vinay Kumar*[1]

[1]*Department of Electrical Engineering, National Institute of Technology Warangal, Warangal, India*

✉ *E-mail: kvpraveenkumar15@gmail.com*

Abstract: Direct torque control (DTC) and predictive torque control (PTC) strategies emerged as powerful tools for speed control of variable frequency drives (VFD). The limitations in classical DTC and PTC are: higher ripple in torque, flux, variable switching frequency, and higher common-mode voltage (CMV). High d*v*/d*t* and CMV results in shaft voltages, bearing currents, malfunction of power electronic devices and electromagnetic interference (EMI). To eliminate the CMVs and also to reduce the switching frequency, voltage vector selection-based DTC and PTC strategies are introduced to an open-end winding induction motor (OEWIM) drive. Another limitation of classical PTC is cumbersome tuning of weighting factors. To address this limitation, modified cost function-based PTC strategy has been developed to eliminate weighting factors. OEWIM drive operates with dual inverter configuration and the two inverters are operated with equal DC-link voltages; therefore, it delivers three-level output voltage. This article introduces various DTC and PTC strategies to an OEWIM drive to reduce torque, flux ripples, switching frequency, elimination of CMV, and weighting factors. The effectiveness of proposed DTC and PTC strategies is tested by dspace-1104 real-time interface controller and comparing the obtained results with classical DTC and PTC.

1 Introduction

Variable frequency drives (VFDs) are popular for speed control of induction motor drives (IMD). To enhance the performance of VFDs, several speed control algorithms came into existence. One of the speed control method to IMDs is direct torque control (DTC). The combination of DTC and model predictive control (MPC) is termed as predictive torque control (PTC). The concept of DTC or PTC strategies is to control stator flux and torque by application of proper voltage vector [1–3]. In general, DTC and PTC strategies are used to trace their reference torque and flux [4]. The hysteresis bounds used in DTC causes current distortions; flux ripple and torque ripple [5]. The implementation of DTC in digital platform needs higher sampling frequencies [6] and leads to develop higher common-mode voltages (CMV). The developed CMV creates shaft voltage through electrostatic coupling. In AC motor drives, electrostatic coupling exists between stator and rotor winding, rotor and frame of the motor. The shaft voltage causes bearing currents, the flow of excessive bearing currents results in premature failure of motor. CMV also causes large common-mode leakage currents. These currents flow back to input terminals and eventually develops common-mode electromagnetic interference (EMI). CMV with high d*v*/d*t* results in bearing currents, shaft voltages, damage of motor bearings, malfunction of power switches, and EMI [6]. In order to operate VFDs efficiently for long durations, it is obvious to eliminate or reduce CMV. There are various methods to reduce CMV: (i) reducing switching frequency [7], (ii) using odd or even switching [8], (iii) making CMV as constant [9], (iv) hardware modifications [10], and (v) using passive filters [11]. In this article, an attempt is made to eliminate CMV with a novel switching state algorithm-based DTC and a simplified cost function-based PTC strategy.

OEWIM drives are best alternative for multi-level inverter-fed induction motors. OEWIM drives have several applications: easy interface with PV arrays [12], hybrid electric vehicles [13], ship propulsion [14], rolling mills etc. OEWIM provides higher redundancy in switching states when compared to neutral point clamped (NPC) inverter configuration. OEWIM can provide two, three, and four-level inversion. By operating the dual inverter configuration of OEWIM with equal DC-link voltages (1:1 ratio), it delivers two- and three-level output voltages. If dual inverter configuration is operated with unequal DC-link voltages (2:1 ratio), four-level inversion can be achieved. The OEWIM configuration has several advantages, when compared with other multi-level inversion (MLI) topologies, such as absence of clamping diodes, needs less number of capacitors, capacitor voltage balance problems do not present [15].

OEWIM drives are more suitable for ship propulsion, electric vehicles, and renewable energy interfacing. The applications like electric vehicles, rolling mills, and other industrial applications require less torque and flux ripples with high dynamic performance. To obtain high dynamic performance, DTC or PTC strategies are preferable. The classical DTC and PTC strategies give higher ripples in torque and flux. Generally, lesser torque and flux ripples can be obtained by using constant switching frequency, duty ratio control, or MLI [16–22]. DTC with constant switching frequencies can be obtained using space vector modulation (SVM). DTC-SVM can reduce torque and flux ripples, but it cannot eliminate the CMV and calculation of timings of active voltage vectors and reference vector location is cumbersome [23]. Duty-ratio-based DTC or PTC [20–22] are based on the concept of application of active voltage vectors and null vectors for certain time intervals. Duty-ratio control algorithm involves calculations of time intervals for active and null vector based on slope of torque error. The generation of reference flux space phasor is cumbersome and duty-ratio-based DTC or PTC cannot eliminate CMV. To reduce torque, flux ripples, and CMV, MLI-fed VFD's are used. CMV in direct torque-controlled IMDs was reported [24], and this DTC strategy utilises active voltage vectors for its operation. DTC strategy used in [24] does not accounts the torque ripple, since it eliminates null vector for its operation. Elimination/reduction of CMV for open-loop configuration of OEWIM configuration was reported [25–28]. DTC and PTC strategies to an OEWIM drive with two-level and more than two-level inversion schemes are reported [29–37]. DTC of OEWIM drive with two-level inversion was reported [29]. Space vector modulation-based DTC strategies are reported in [30, 31]. In [30], DTC of OEWIM drive implemented for ship propulsion with SVM technique. Five-level inversion-based space vector modulated DTC strategy introduced

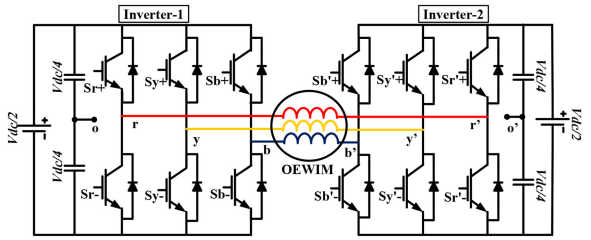

Fig. 1 *Dual inverter fed OEWIM drive*

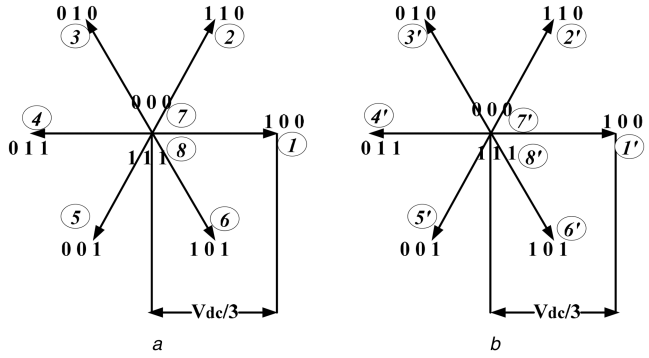

Fig. 2 *Space vector locations*
(a) Inverter-1 and, ***(b)*** Inverter-2

for an OEWIM drive [31]. In [32, 33], effective voltage switching state algorithms introduced to an OEWIM drive for three-level and four-level inversion, the modified look-up tables utilises rotor speed. PTC of OEWIM drive with equal and unequal DC-link voltages are reported in [34–37]. In [16, 34, 37], PTC of OEWIM has been introduced to reduce zero-sequence currents and CMV, but these strategies utilises weighting factor for its operation. In [34], PTC of OEWIM was introduced with two, three, and four-level inversion schemes, but the PTC strategies used in this article uses modified cost function, predefined set of voltage space vectors based on rotor speed and complex tuning of weighting factors. In [35], weighting factor elimination-based PTC strategy was introduced by considering flux space vector in the cost function and it also states that if the cost function comprises of more than two control objectives, then weighting factors are unavoidable. Self-tuning of weighting factors was introduced for OEWIM for four-level inversion [36], but it cannot reduce ripples in torque and flux in addition it increases computational burden on controller. The effects of dead-time effects to eliminate CMV for OEWIM drive with three-level inversion have been addressed [38].

This article introduces enhanced voltage switching algorithm, simplified cost function-based DTC and PTC strategies for an OEWIM drive. The DTC and PTC strategies used in this article provide all features of classical PTC and DTC strategies. The proposed PTC algorithms do not involve complex equations to reduce switching frequency. Another limitation of classical PTC strategy is tuning of weighting factors. To address the problem of weighting factor, modified cost function is used. The modified cost function comprises of active torque and reactive torque components as control objectives. The intents of this article are: (i) developing discrete models of dual inverter configuration and OEWIM drive, (ii) implementing simplified voltage switching state algorithm to eliminate CMV, (iii) modified hysteresis controller-based DTC strategy to an OEIWM with three-level inversion, (iv) introduces a simple weighting factor elimination-based PTC strategy for OEWIM with three-level inversion (v) elimination of CMV, weighting factors in DTC and PTC strategies (vi) reduction of dead time effects and (vii) reduction of switching frequency.

The proposed algorithms are implemented to OEWIM, by considering the inverters are operating with equal DC-link voltages. In this configuration, OEWIM has 64 switching states. Out of these 64 switching states, there are 12 voltage space vector locations which provide '$\pm 1/6$' of effective DC-link voltage as CMV and seven voltage vectors provide zero CMV. The proposed DTC/PTC strategies are implemented with simplified switching state algorithms for OEWIM drive with two-level and three-level inversion.

In this article, one-step prediction algorithm is used to implement PTC of OEWIM drive by considering discrete model of dual inverter and OEWIM drive. The structure of this article is as follows. Section II describes power circuit configuration and discrete model of OEWIM drive. Section III discusses implementation of two-level DTC of OEWIM drive with CMV (DTC-I), three-level DTC of OEWIM (DTC-II) and DTC of OEIWM drive without CMV (DTC-III). Section IV focuses on implementation of PTC of OEWIM with CMV (PTC-I), weighting factor eliminated PTC (PTC-II) and PTC of OEWIM without CMV and reducing switching frequency (PTC-III). Section V is to prove the effectiveness of the proposed algorithms by implementing in real time with dspace DS-1104 controller. The obtained simulation and experimental results are compared with classical two-level DTC of OEWIM drive.

2 Power circuit and dynamic model of OEWIM

2.1 Configuration of dual inverter fed OEWIM drive

The configuration of dual inverter fed OEWIM drive is shown in Fig. 1. It comprises of two two-level voltage source inverters and those are operated with equal DC-link voltages. The space vector locations of inverter-1 and inverter-2 are given by (1–8) and (1'–8') shown in Fig. 2. By operating the two inverters with '$V_{dc}/2$', each inverter provides six active vector locations and two null vectors. Two inverters provide 64 switching states. OEWIM is rich in redundancy of switching states; hence, it provides 18 active voltage vectors and a null vector (V_0) as shown in Fig. 3*a*. These vectors are classified into three categories; these are high (V_{21}–V_{26}), intermediate (V_{11}–V_{16}), and low-voltage vectors (V_1–V_6). High-voltage vectors (V_{21}–V_{26}) are used in DTC-I, PTC-I, whereas intermediate voltage vectors (V_{11}–V_{16}) used for DTC-III, PTC-III. In contrary, DTC-II and PTC-II are formulated by considering 19 voltage space vector combinations. Realisation of these 19 voltage space vectors and their switching combinations are shown in Table 1. Fig. 3*a*, represents voltage space vector locations of dual inverter configuration and Fig. 3*b* represents classification of sectors used in DTC-II. The pole voltages of inverter-1 and inverter-2 are represented by (V_{ro}, V_{yo}, V_{bo}) and ($V_{r'o'}$, $V_{y'o'}$, $V_{b'o'}$). Pole voltages of inverters are given by (1) and (2).

$$\begin{pmatrix} V_{ro} \\ V_{yo} \\ V_{bo} \end{pmatrix} = \begin{cases} V_{dc}/4 \text{ when } S_r = S_y = S_b = 1 \\ -V_{dc}/4 \text{ when } S_r = S_y = S_b = 0 \end{cases} \tag{1}$$

$$\begin{pmatrix} V_{r'o'} \\ V_{y'o'} \\ V_{b'o'} \end{pmatrix} = \begin{cases} V_{dc}/4 \text{ when } S_{r'} = S_{y'} = S_{b'} = 1 \\ -V_{dc}/4 \text{ when } S_{r'} = S_{y'} = S_{b'} = 0 \end{cases} \tag{2}$$

To determine the phase voltages of inverters, it is necessary to determine difference of pole voltages (3) and CMV (4).

$$\begin{pmatrix} \delta V_{rr'} \\ \delta V_{yy'} \\ \delta V_{bb'} \end{pmatrix} = \begin{pmatrix} V_{ro} - V_{r'o'} \\ V_{yo} - V_{y'o'} \\ V_{bo} - V_{b'o'} \end{pmatrix} \tag{3}$$

The CMV of OEWIM drive is determined between the points 'o' and 'o'' [15].

$$V_{oo'} = \frac{1}{3}(\delta V_{rr'} + \delta V_{yy'} + \delta V_{bb'}) \tag{4}$$

The phase voltages of OEWIM drive are obtained by subtracting (3) and (4). The phase voltages of OEWIM are given by (5) and (6) represents simplified form of phase voltages of OEWIM drive [15].

$$\begin{pmatrix} V_{rr'} \\ V_{yy'} \\ V_{bb'} \end{pmatrix} = \begin{pmatrix} \delta V_{rr'} \\ \delta V_{yy'} \\ \delta V_{bb'} \end{pmatrix} - \begin{pmatrix} V_{oo'} \\ V_{oo'} \\ V_{oo'} \end{pmatrix} \tag{5}$$

$$\begin{pmatrix} V_{rr'} \\ V_{yy'} \\ V_{bb'} \end{pmatrix} = \frac{1}{3}\begin{pmatrix} 2 & -1 & -1 \\ -1 & 2 & -1 \\ -1 & -1 & 2 \end{pmatrix}\begin{pmatrix} \delta V_{rr'} \\ \delta V_{yy'} \\ \delta V_{bb'} \end{pmatrix} \tag{6}$$

The output voltages of inverter-1 & 2 are given by (7) & (8), (9) represents resultant voltage vector [34]. Fig. 3*a* represents voltage vectors of OEWIM drive corresponding to switching states shown in Table 1.

$$V_{s1} = \left(\frac{2}{3}\right)\left(\frac{V_{dc}}{2}\right)\left(S_r + S_y e^{j(2\pi/3)} + S_b e^{-j(2\pi/3)}\right) \tag{7}$$

$$V_{s2} = \left(\frac{2}{3}\right)\left(\frac{V_{dc}}{2}\right)\left(S'_r + S'_y e^{j(2\pi/3)} + S'_b e^{-j(2\pi/3)}\right) \tag{8}$$

And

$$V_{sr} = V_{s1} - V_{s2} \tag{9}$$

2.2 Dynamic model of OEWIM drive

The dynamic model of OEWIM drive used for simulation and experimental verification is shown in Fig. 4. The dynamic

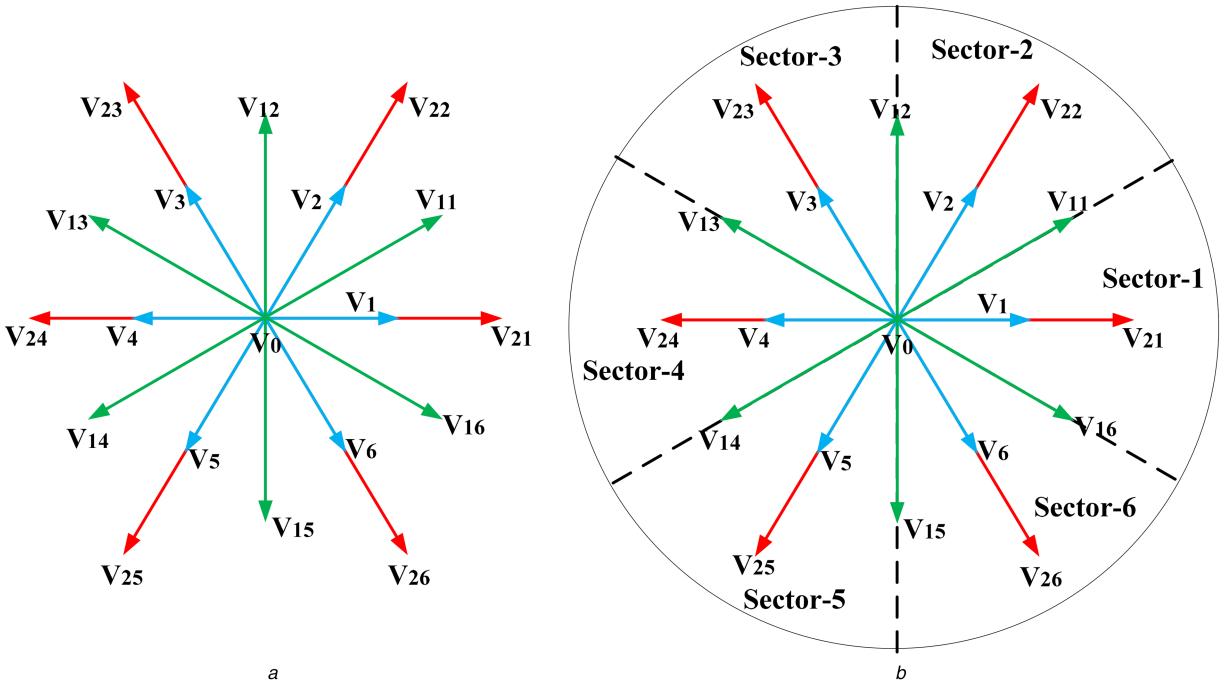

Fig. 3 *Voltage space vector locations of dual inverter configuration with three-level inversion*
(a) Classification of voltage space vectors and, ***(b)*** Classification of sectors

Table 1 CMV and Realisation of voltage space vectors of dual inverter fed OEWIM drive

VSI-1 (S_{ryb})	VSI-2 ($S_{r'y'b'}$)	CMV V_o	Realisation	Voltage Vector	
			V_α	V_β	*Vsr*
0 0 0	0 0 0	0	0	0	V_0
1 1 0	0 1 0	$V_{dc}/6$	$0.33\times V_{dc}$	0	V_1
0 1 0	0 1 1	$-V_{dc}/6$	$0.167\times V_{dc}$	$0.28\times V_{dc}$	V_2
0 1 1	0 0 1	$V_{dc}/6$	$-0.16\times V_{dc}$	$0.28\times V_{dc}$	V_3
0 0 1	1 0 1	$-V_{dc}/6$	$-0.33\times V_{dc}$	0	V_4
1 0 1	1 0 0	$V_{dc}/6$	$-0.16\times V_{dc}$	$-0.28\times V_{dc}$	V_5
1 0 0	1 1 0	$-V_{dc}/6$	$0.167\times V_{dc}$	$-0.28\times V_{dc}$	V_6
1 0 0	0 0 1	0	$0.5\times V_{dc}$	$0.28\times V_{dc}$	V_{11}
0 1 0	0 0 1	0	0	$0.57\times V_{dc}$	V_{12}
0 1 0	0 1 1	0	$-0.5\times V_{dc}$	$0.28\times V_{dc}$	V_{13}
0 0 1	0 1 1	0	$-0.5\times V_{dc}$	$-0.28\times V_{dc}$	V_{14}
0 0 1	0 1 0	0	0	$-0.5\times V_{dc}$	V_{15}
1 0 0	0 1 0	0	$0.5\times V_{dc}$	$-0.28\times V_{dc}$	V_{16}
1 0 0	0 1 1	$-V_{dc}/6$	$0.667\times V_{dc}$	0	V_{21}
1 1 0	0 0 1	$V_{dc}/6$	$0.33\times V_{dc}$	$0.57\times V_{dc}$	V_{22}
0 1 0	1 0 1	$-V_{dc}/6$	$-0.33\times V_{dc}$	$0.57\times V_{dc}$	V_{23}
0 1 1	1 0 0	$V_{dc}/6$	$-0.67\times V_{dc}$	0	V_{24}
0 0 1	1 1 0	$-V_{dc}/6$	$-0.33\times V_{dc}$	$-0.57\times V_{dc}$	V_{25}
1 0 1	0 1 0	$V_{dc}/6$	$0.33\times V_{dc}$	$-0.57\times V_{dc}$	V_{26}

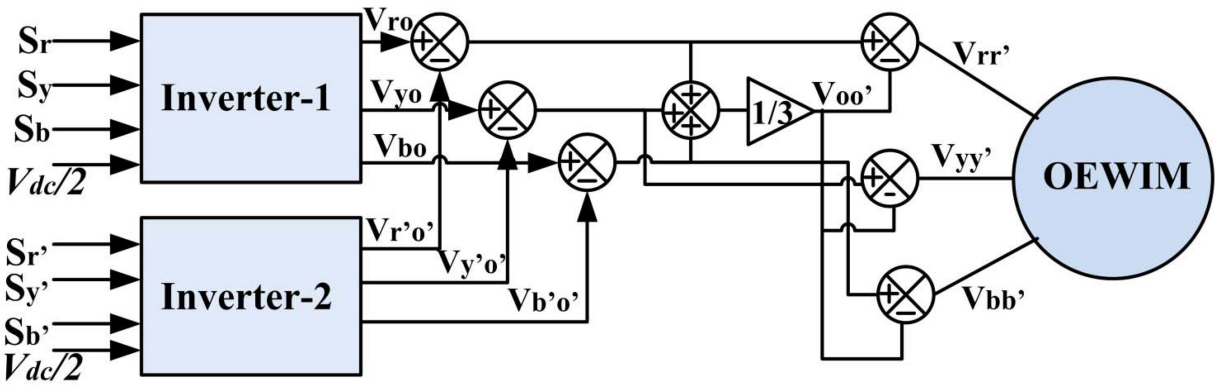

Fig. 4 *Configuration of OEWIM drive in stationary reference frames*

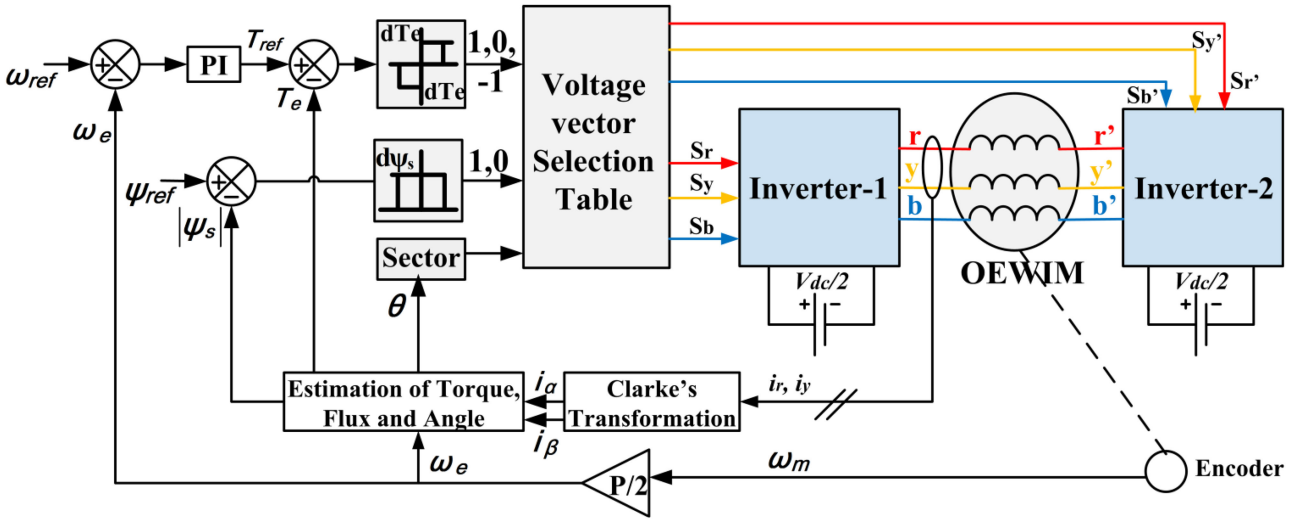

Fig. 5 *DTC strategy of dual inverter fed OEWIM drive*

equations used for DTC and PTC of OEWIM are given by (10)–(15). The stator and rotor voltage equations in complex form are given by (10) and (11).

$$V_s = R_s i_s + p\psi_s \tag{10}$$

$$0 = R_r i_r + p\psi_r - j\omega_e \psi_r \tag{11}$$

Stator and rotor flux linkage of OEWIM is given by (12) and (13).

$$\psi_s = L_s i_s + L_m i_r \tag{12}$$

$$\psi_r = L_r i_r + L_m i_s \tag{13}$$

The electromagnetic torque of OEWIM is obtained by using (10)–(13). The torque of OEWIM drive is given by (14)

$$T_e = \frac{3}{2}\frac{P}{2}\text{imag}(\psi_s^* i_s) \tag{14}$$

Mechanical equation of OEWIM is used to find the speed. From (14) the mechanical speed of OEWIM can be written as (15).

$$J\frac{d\omega_m}{dt} = (T_e - T_l) \tag{15}$$

In (10)–(15), suffix 's' refers to stator quantities, suffix 'r' refers to rotor quantities, 'R' represents resistance, 'L' represents self-inductance, 'L_m' represents magnetising inductance, 'i' represents current, 'ψ' represents flux linkages, 'V_s' represents stator voltage, 'P' represents number of poles, 'T_e' represents electromagnetic torque, 'T_l' represents load torque applied on to the shaft of motor 'ω_e' represents angular speed of rotor in electrical systems (rad/s) and 'ω_m' represents mechanical speed of rotor in mechanical systems (rad/s).

3 Proposed direct torque control strategies

3.1 DTC of OEWIM with CMV (DTC-I)

The block diagram used to implement DTC-I is shown in Fig. 5. The block diagram comprises of two inverters operating in dual mode, speed encoder, estimator to find torque, flux and angle. DTC-I is implemented by using three-level torque hysteresis controller and two-level flux hysteresis controller. The output of hysteresis controllers and sector identifier are used to select the voltage vector to be applied for inverters. The selection of voltage vector plays a vital role on the operation of OEWIM drive. The switching states used in DTC-I are given in Table 1 (V_0, V_{21}–V_{26}). The CMV corresponding to each switching state used in DTC-I is also described in Table 1. The switching states used to implement proposed DTC strategy develops less CMV [24].

Fig. 6*a* represents voltage space vectors used for DTC-I, whereas Fig. 6*b* represents classification of sectors and each sector is distributed with an angle of 60°. After finding location of active voltage vectors and sector identification, it is easy to find voltage vector to be applied for operation of OEWIM drive [29]. The selection of voltage vector is shown in Table 2. The choice of voltage vector should provide dynamic changes of torque and flux. By applying proper voltage vector the output voltage of dual inverter fed OEWIM can be varied. The voltage vector should maintain less distortion in current. If the distortions in current are less, it leads to fewer ripples in torque and flux. From (14), torque of OEWIM depends on stator flux and stator current. As the time constant of rotor is high when compared with stator, hence rotor flux is assumed to be constant. Dynamic performance of OEWIM

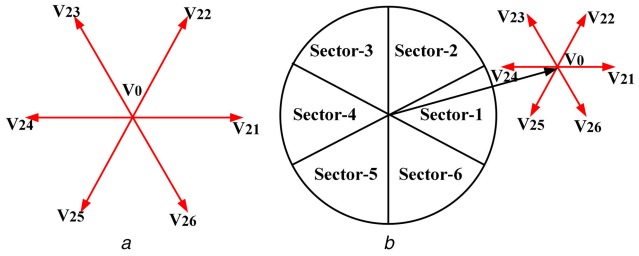

Fig. 6 *Classification of active voltage vectors*
(a) Locations of full voltage vectors and, ***(b)*** Sector classification

Table 2 Voltage vector selection table for DTC-I

Flux Error	Torque Error	Sector					
$d\psi_s$	dT_e	1	2	3	4	5	6
1	1	V_{22}	V_{23}	V_{24}	V_{25}	V_{26}	V_{21}
	0	V_0	V_0	V_0	V_0	V_0	V_0
	−1	V_{26}	V_{21}	V_{22}	V_{23}	V_{24}	V_{25}
0	1	V_{23}	V_{24}	V_{25}	V_{26}	V_{21}	V_{22}
	0	V_0	V_0	V_0	V_0	V_0	V_0
	−1	V_{25}	V_{26}	V_{21}	V_{22}	V_{23}	V_{24}

Table 3 Impact of Voltage Space Vectors on Dynamic Characteristics of OEWIM drive for DTC-I and PTC-I

	V_0	V_{21}	V_{22}	V_{23}	V_{24}	V_{25}	V_{26}
flux (ψ_s)	0	↑↑↑	↑↑	↓	↓↓↓	↓↓	↑
torque (T_e)	0	↓	↑↑	↑↑↑	↑	↓↓	↓↓↓

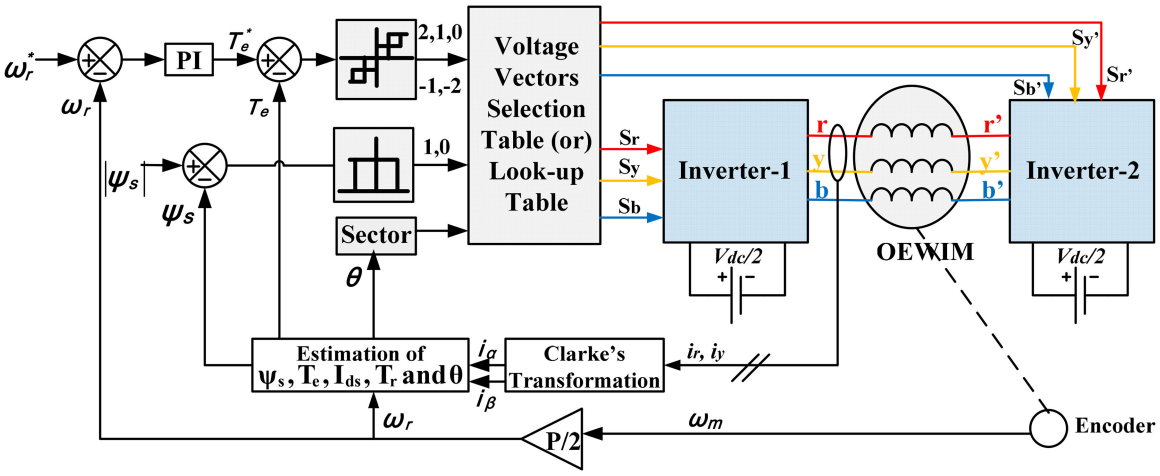

Fig. 7 *DTC of OEWIM drive with three-level inversion*

drive is influenced by stator flux and current [39]. To obtain dynamic variation in torque and flux specified voltage vector should be applied as shown in Table 2. The influence of the voltage vector on performance of OEWIM drive by considering the stator flux is in sector-I and it is shown in Table 3. In Table 3, ↑ represents increment and ↓ decrement.

3.2 DTC of OEWIM drive with three-level inversion (DTC-II)

DTC of OEWIM drive with three-level inversion is shown in Fig. 7. The same principle of classical DTC (DTC-I) can be extendible for three-level inversion. The voltage space vectors for three-level inversion is shown in Table 1. The voltage vectors in DTC-I are six active voltage vectors and a null vector; therefore, six sectors are used. In DTC of OEWIM drive with three-level inversion there exist 18 active voltage vectors and a null vector, hence it needs modifications from DTC-I. The proposed DTC strategy utilises a five-level torque hysteresis controller, two-level flux hysteresis controller and sector identifier. In DTC-I, to utilise the voltage vectors six sectors are used. In DTC-II, 12 sectors are used and each sector is divided with an angle of 30°.

The voltage vector selection table for DTC-II is given by Table 4. In Table 4, it is identified that flux error varies between zero and one, whereas torque error varies in the range of ± 2. The voltage vectors are selected by torque error and flux error, if the torque error is ± 2, then intermediate (V_{11}–V_{16}) and high-voltage vectors (V_{21}–V_{26}) are used. If the torque error is ± 1, then low-voltage vectors (V_1–V_6) are used and the selection of voltage vectors is same as DTC-I. The proposed DTC strategy is very simple, since it uses a simple five-level torque hysteresis controller and a two-level flux hysteresis controller. The effect of voltage vectors on torque and flux ripple is same as DTC-I shown in Table 3.

3.3 DTC of OEWIM drive without CMV (DTC-III)

The block diagram used to implement DTC-III is shown in Fig. 5. To implement DTC-III intermediate voltage vectors (V_{11}–V_{16}) are

Table 4 Voltage vector selection table for DTC-II

Flux Error	Torque Error	Sector											
$d\psi_s$	dT_e	1	2	3	4	5	6	7	8	9	10	11	12
1	2	V_{22}	V_{12}	V_{23}	V_{13}	V_{24}	V_{14}	V_{25}	V_{15}	V_{26}	V_{16}	V_{21}	V_{11}
	1	V_2	V_2	V_3	V_3	V_4	V_4	V_5	V_5	V_6	V_6	V_1	V_1
	0	V_0	V_0	V_0	V_0	V_0	V_0	V_0	V_0	V_0	V_0	V_0	V_0
	−1	V_6	V_6	V_1	V_1	V_2	V_2	V_3	V_3	V_4	V_4	V_5	V_5
	−2	V_{26}	V_{16}	V_{21}	V_{11}	V_{22}	V_{12}	V_{23}	V_{13}	V_{24}	V_{14}	V_{25}	V_{15}
0	2	V_{23}	V_{13}	V_{24}	V_{14}	V_{25}	V_{15}	V_{26}	V_{16}	V_{21}	V_{11}	V_{22}	V_{12}
	1	V_3	V_3	V_4	V_4	V_5	V_5	V_6	V_6	V_1	V_1	V_2	V_2
	0	V_0	V_0	V_0	V_0	V_0	V_0	V_0	V_0	V_0	V_0	V_0	V_0
	−1	V_5	V_5	V_6	V_6	V_1	V_1	V_2	V_2	V_3	V_3	V_4	V_4
	−2	V_{25}	V_{15}	V_{26}	V_{16}	V_{21}	V_{11}	V_{22}	V_{12}	V_{23}	V_{13}	V_{24}	V_{14}

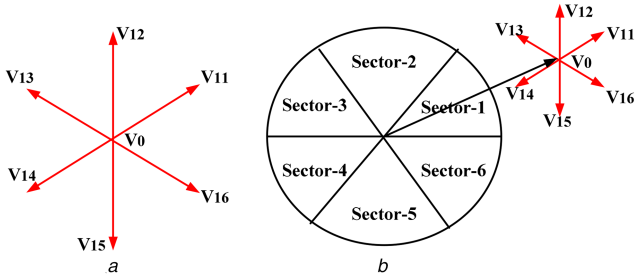

Fig. 8 *Classification of active voltage vectors*
(a) Locations of intermediate voltage vectors and, ***(b)*** Sector classification

Table 5 Voltage vector selection table for DTC-III

Flux Error	Torque Error	Sector					
$d\psi_s$	dT_e	1	2	3	4	5	6
1	1	V_{12}	V_{13}	V_{14}	V_{15}	V_{16}	V_{11}
	0	V_0	V_0	V_0	V_0	V_0	V_0
	−1	V_{16}	V_{11}	V_{12}	V_{13}	V_{14}	V_{15}
0	1	V_{13}	V_{14}	V_{15}	V_{16}	V_{11}	V_{12}
	0	V_0	V_0	V_0	V_0	V_0	V_0
	−1	V_{15}	V_{16}	V_{11}	V_{12}	V_{13}	V_{14}

Table 6 Impact of voltage vectors on dynamic characteristics of OEWIM drive for DTC-III and PTC-III

	V_0	V_{11}	V_{12}	V_{13}	V_{14}	V_{15}	V_{16}
flux (ψ_s)	0	↑↑↑	↑↑	↓	↓↓↓	↓↓	↑
torque (T_e)	0	↓	↑↑	↑↑↑	↑	↓↓	↓↓↓

used to eliminate CMV and dead-time effects by allowing a current flow path [38]. The location of intermediate voltage vectors are shown in Fig. 8. The proposed DTC-III strategy works on the same principle of DTC-I except two modifications.

The modifications are: (i) classification of sectors and (ii) selection of active voltage vectors. In DTC-III, the sectors are distributed with 60° and sector-1 is from 0 to 60^0, whereas in DTC-I sector-1 is from −30 to 30^0.

The location of active voltage vectors used to implement DTC-III is shown in Figs. 8*a* and *b* represents classification of sectors used in DTC-III. The intermediate voltage vectors (V_{11}–V_{16}) to eliminate CMV and their realisation are shown in Table 1.

The selection of voltage vectors used in DTC-III strategy is shown in Table 5. The influence of voltage vectors on the performance of OEWIM by assuming flux space phasor in Sector-1 is shown in Table 6. The voltage vectors used in DTC-III are intermediate voltage vectors; therefore, these voltage vectors gives zero CMV.

4 Proposed predictive torque control strategies

4.1 PTC of OEWIM drive with CMV (PTC-I)

The block diagram to implement PTC of OEWIM drive is shown in Fig. 9. Operating principle of PTC is same as DTC. In PTC, the reference values of control variables are compared with predicted variables. The cost function is used to make comparison between reference and predicted variables. The proposed PTC strategy can be implemented with the following steps: (i) Find the variables which can be directly measurable, (ii) Estimate the variables which cannot be measurable, (iii) Predict the control variables from measurements and estimates, (iv) Formulate the cost function and (v) Minimise the cost function to generate the switching pulses [34].

To implement the proposed PTC strategy speed, DC-link voltage, and stator currents are used as measurements. Flux and torque are considered as control variables, and these are estimated at kth instant by using measurements. The prediction of control variables at $(k+1)$ instant is obtained by (16)–(21); hence, one-step ahead prediction horizon is used. The optimisation of cost function is considered for the switching states of dual inverter configuration shown in Fig. 6*a*, for high-voltage vectors (V_0, V_{21}–V_{26}). The

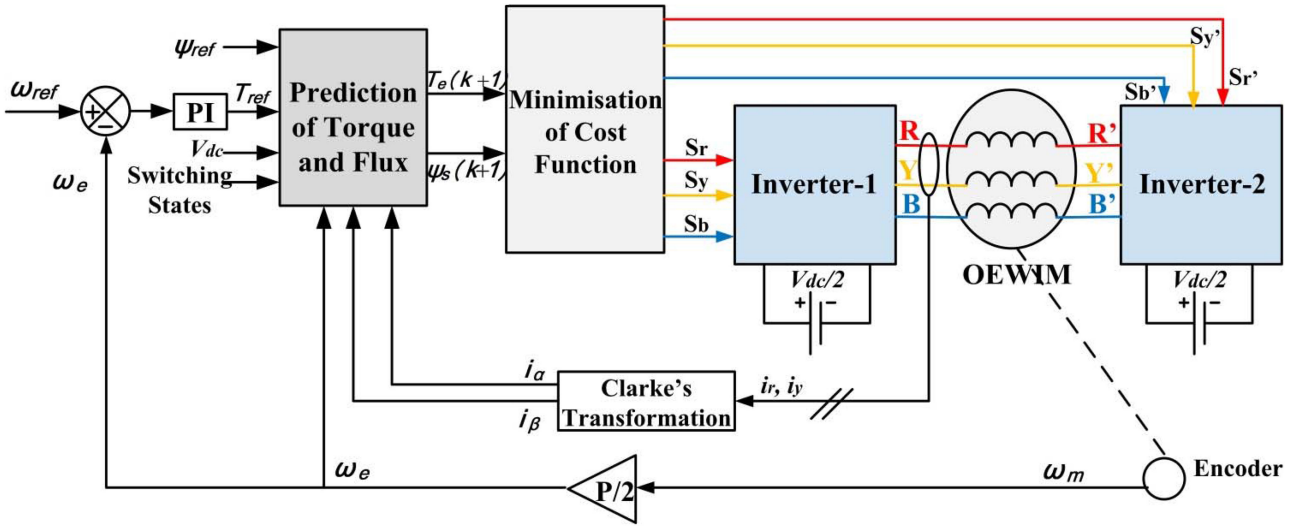

Fig. 9 *PTC strategy of dual inverter fed OEWIM drive*

switching combinations of dual inverter configuration for high voltage vectors are shown in Table 1. For these switching states, the cost function is evaluated and the switching state which delivers minimum amount of torque and flux ripple can be chosen as optimum voltage vector.

To predict torque and flux of OEWIM drive Eulers forward differentiation is used. Forward Eulers approach is given by (16).

$$\frac{\mathrm{d}x}{\mathrm{d}t} = \frac{x(k+1)-x(k)}{T_s} \Rightarrow x(k+1) = \frac{\mathrm{d}x}{\mathrm{d}t}T_s + x(k) \tag{16}$$

Here, 'T_s' indicates sample time.

The predicted flux is obtained from (7) and it is given by

$$\frac{\mathrm{d}\psi_s(k)}{\mathrm{d}t} = V_s(k) - R_s i_s(k) \tag{17}$$

$$\psi_s(k+1) = (V_s - R_s i_s)T_s + \psi_s(k) \tag{18}$$

On simplifying (10)–(13), stator current in state variable form can be written as

$$\frac{\mathrm{d}i_s(k)}{\mathrm{d}t} = A_1(V_s(k) - A_2 i_s(k) + A_3\psi_s(k) - j\omega_e\psi_r A_4) \tag{19}$$

From (19), the predicted stator current is given by

$$i_s(k+1) = T_s(A_1(V_s(k) - A_2 i_s(k) + A_3\psi_s(k) - j\omega_e\psi_r A_4)) + i_s(k) \tag{20}$$

Here, $A_1 = \dfrac{L_r}{L_s L_r - L_m^2}$; $A_2 = R_s + \dfrac{L_s R_r}{L_r}$; $A_3 = \dfrac{R_r}{L_r}$ and $A_4 = \dfrac{L_m}{L_r}$. The electromagnetic torque (14) of OEWIM is dependent on stator flux and stator current. If the predicted stator flux and currents are known then it is easy to find electromagnetic torque at $(k+1)$ instant.

$$T_e(k+1) = \frac{3}{2}\frac{P}{2}\mathrm{imag}(\psi_s^*(k+1)i_s(k+1)) \tag{21}$$

If the control variables are determined at $(k+1)$ instant, then it is easy to formulate cost function and it is described by (22).

$$f = |T_{\mathrm{ref}} - T(k+1)| + \sigma|\psi_{\mathrm{ref}} - \psi_s(k+1)| \tag{22}$$

In (22), 'T_{ref}' indicates torque reference, 'ψ_{ref}' is stator flux reference and 'σ' is weighting factor of flux [19].

From (18) and (20) the stator flux and stator current are dependent on output voltage of inverter $V_s(k)$, hence these are predicted for seven switching states shown in Fig. 6*a*. Finally, the selection of switching state is done by minimisation of cost function [34]. The cost function contains the control law, in (21) the cost function is used to control torque and stator flux of OEWIM drive. The cost function is evaluated for seven switching combinations and the switching state which gives lowest value is selected as optimal switching state and thus drives the inverters. The weighting factor 'σ' used in PTC-I is '75' [34].

4.2 Weighting factor eliminated PTC of OEWIM drive with three-level inversion (PTC-II)

From PTC-I, it is evident that the cost function comprises of weighting factor 'σ', tuning of weighting factor is difficult. The choice of 'σ' affects the performance of OEWIM drive. There are several methods available to tune the weighting factors. In [34, 37], branch and bound algorithm was used to tune weighting factor. In this article, a simplified PTC strategy has been developed by modifying the cost function in such a way that it does not use weighting factors. The block diagram of PTC-II is shown in Fig. 10. The steps used to develop PTC-II are same as PTC-I, except that it uses a modified cost function.

$$f = |T_{\mathrm{ref}} - T(k+1)| + |T_{R\mathrm{ref}} - T_R(k+1)| \tag{23}$$

The cost function used in PTC-II is given by (23), in (23) '$T_{R\mathrm{ref}}$' indicates reactive torque reference and '$T_R(k+1)$' is reactive torque at $(k+1)$ instant.

For an OEWIM, drive reactive torque T_R is given by (24),

$$T_R = \frac{3}{2}\frac{P}{2}\mathrm{real}(\psi_s^* i_s) \tag{24}$$

If the reactive torque is known [39], in discrete form reactive form at $(k+1)$ instant is given by (25).

$$T_R(k+1) = \frac{3}{2}\frac{P}{2}\mathrm{real}(\psi_s^*(k+1)i_s(k+1)) \tag{25}$$

The cost function (23) is evaluated for all voltage space vector combinations of dual inverter configuration shown in Table 1. The electromagnetic torque $T(k+1)$ and $T_R(k+1)$ are evaluated for all 19 space vector locations. Out of these 19 space vector combination, the optimal switching state is selected for the minimum value of cost function (23). The cost function used in PTC-II comprises of electromagnetic torque and reactive torque; therefore; PTC-II is free from weighting factors.

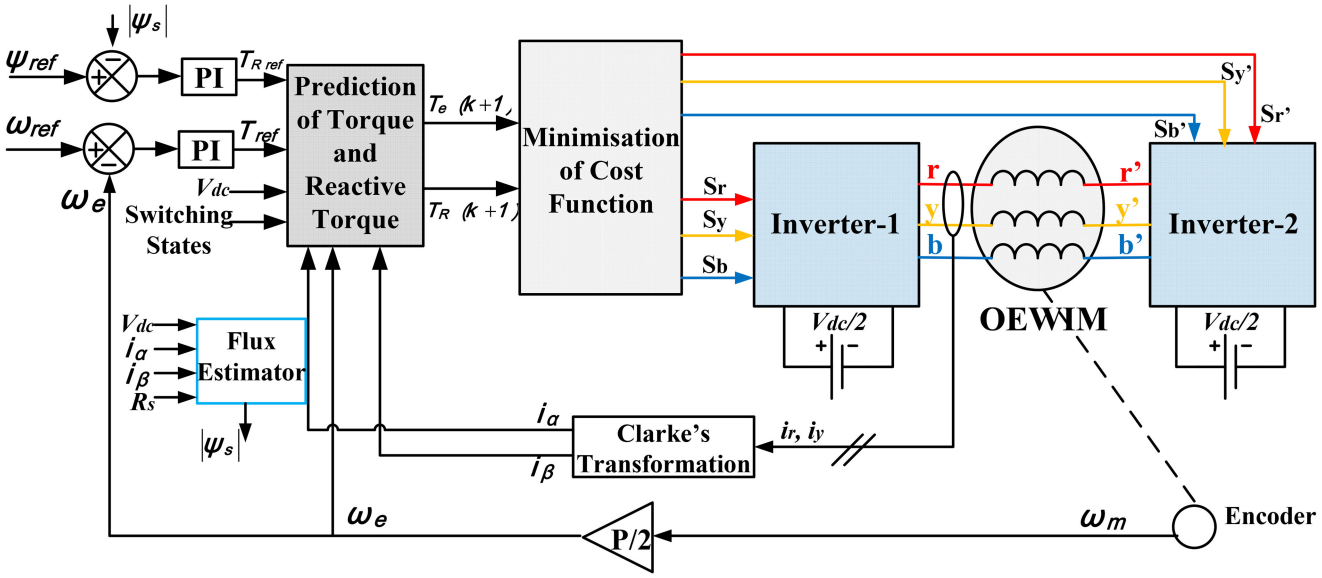

Fig. 10 *PTC strategy of OEWIM drive with three-level inversion*

4.3 PTC of OEWIM drive without CMV and reduced switching frequency (PTC-III)

In the above section, weighting factor eliminated PTC strategy has been introduced to an OEWIM drive. The cost function in PTC-II comprises of electromagnetic torque and reactive torque components; therefore, PTC-II cannot reduce switching frequency and do not eliminate CMV. To eliminate CMV and also to reduce switching frequency, selective voltage vector-based PTC strategy (PTC-III) is introduced. The block diagram of PTC-III is shown in Fig. 10. Intermediate voltage vectors (V_{11}–V_{16}) are used to develop PTC-III strategy and these voltage vectors are shown in Table 1. The cost function (26) used to implement PTC-III comprises of three control objectives. The control objectives are: (i) torque error reduction (ii) flux error reduction/reactive torque error reduction, and (iii) reduction of switching frequency. In PTC of OEWIM drives, the switching frequency is very high; hence, it is important to reduce switching frequency. By reducing the switching frequency number of commutations of power switches can be reduced. To reduce number of commutations, the voltage space vector at $(k+1)$ and kth instants are used.

$$f = |T_{\text{ref}} - T_{\text{e}}(k+1)| + |T_{R\text{ref}} - T_R(k+1)| + \lambda|V_s(k+1) - V_s(k)| \tag{26}$$

In (23), $V_s(k+1)$ and $V_s(k)$ are the voltage vectors at $(k+1)$ instant and kth instant. The switching frequency of OEWIM drive can be reduced by controlling number of switch transitions. The cost function (23) is evaluated for the voltage space vectors shown in Fig. 8. The voltage vector which gives minimum torque ripple and switching frequency used as optimal voltage vector and applied in next control interval. In (26), 'λ' is weighting factor of switching frequency. The weighting factor is chosen empirically. In order to achieve desired performance of the OEWIM drive, several offline simulations are performed. To obtain desired performance the weighting factors are tuned by observing several offline simulations, finally it has been observed that the OEWIM gives good response for $\lambda = (1/V_{\text{dc}}) = 0.0018$ [16, 19, 34].

5 Simulation and experimental results

The proposed DTC and PTC strategies shown in Figs. 5, 7, 9, and 10 are developed in MATLAB. To validate the effectiveness of the DTC and PTC algorithms, the proposed algorithms are developed with dspace DS-1104 controller. The parameters used for simulation and experimentation are shown in Table 7. The effectiveness of proposed algorithms (DTC-II, DTC-III, PTC-II and PTC-III) is verified by comparing the simulated and experimental results with DTC-I, PTC-I and other control strategies [24, 32, 34].

Table 7 Specifications of OEWIM drive

Motor Parameter	Value
stator resistance (R_S)	4.2 Ω
rotor resistance (R_r)	6.27 Ω
stator inductance (Ls)	0.54 H
rotor inductance (Lr)	0.54 H
mutual inductance (Lm)	0.512 H
poles (P)	4
rated power (P_n)	3.7 kW
rated speed (rpm)	1440
rated torque (Nm)	24.48
rated flux (Wb)	1
inertia (J)	0.051 kg.m^2

5.1 Simulation results

The simulation studies are performed by implementing proposed strategies in MATLAB/SIMULINK. The dual inverter fed OEWIM drive is modelled mathematically by using (10)–(15) in simulink. The inverters are operated with equal DC-link voltage of 270 V, with an effective DC-link voltage of 540 V (V_{dc}). To verify the effectiveness of the proposed algorithms, the OEWIM drive is subjected to operate at different operating speeds. In interest of brevity, the simulation results are shown for step change in speed variation from forward motoring to reverse motoring.

Figs. 11 and 12 demonstrates simulated response of OEWIM drive for the step change in speed variation from 250– −250 rad/s. Fig. 11 represents simulated response of DTC-I, DTC-II and DTC-III. Fig. 12 represents simulated response of PTC-I, PTC-II and PTC-III. Initially OEWIM drive is operating at 250 rad/s (forward motoring), at the simulation time of 2 seconds step change in speed of −250 rad/s (reverse motoring) is applied to OEWIM drive. When the step change in speed applied to OEWIM drive, the speed settled at 2.12 s. After 2.12 seconds the OEIWM drive is operating at a steady speed of −250 rad/s.

From Figs. 11*a* and 12*a* PTC-I develops fewer torque and flux ripples when compared with DTC-I. From Figs. 11*b* and 12*b*, it is clear that the torque, flux ripples of OEWIM drive are less in PTC-II when compared with DTC-II. From Fig. 11*c* and 12*c* it is also clear that PTC-III delivers higher torque ripples when compared with PTC-II and lesser ripples when compared with PTC-I whereas switching frequency of PTC-III is less than that of PTC-I and PTC-II. From Figs. 11*b*, *c*, 12*b* and *c* it is observed that the proposed

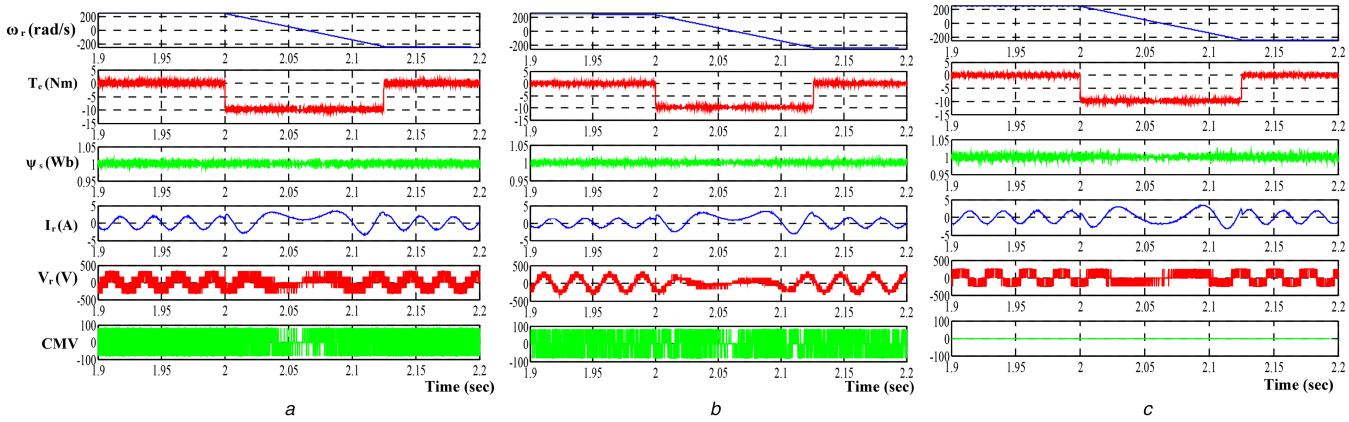

Fig. 11 *Simulation response of speed, torque, flux, current, voltage and CMV of OEWIM drive during forward motoring to reverse motoring*
(a) DTC-I, ***(b)*** DTC-II and, ***(c)*** DTC-III

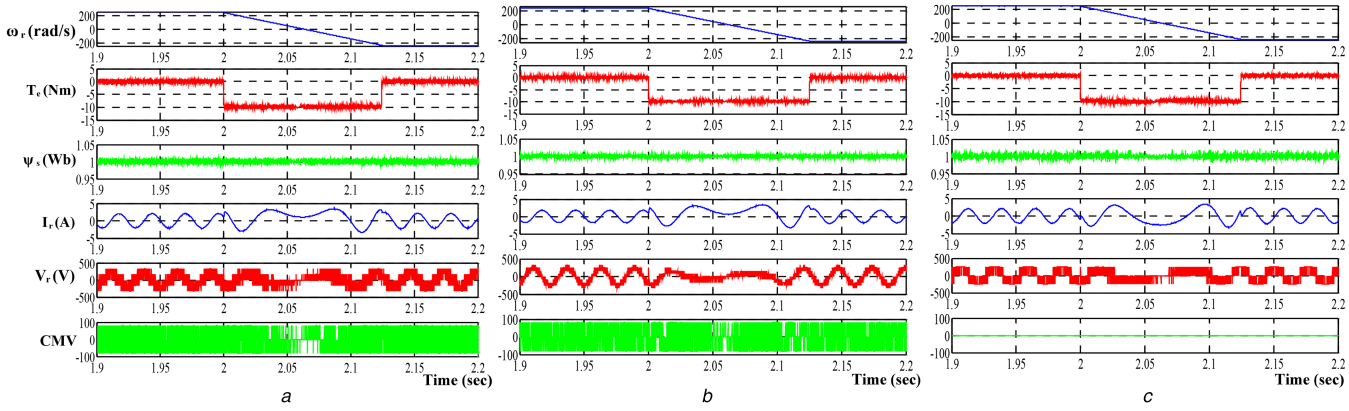

Fig. 12 *Simulation response of speed, torque, flux, current, voltage and CMV of OEWIM drive during forward motoring to reverse motoring*
(a) PTC-I, ***(b)*** PTC-II and, ***(c)*** PTC-III

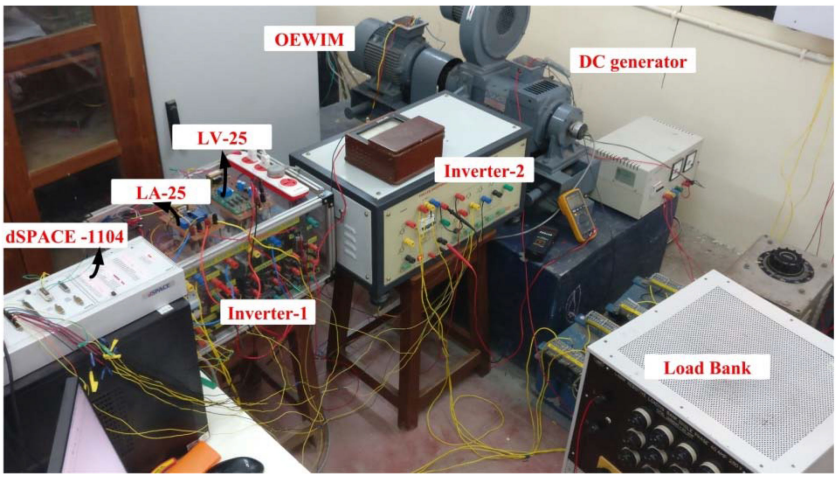

Fig. 13 *Test Bench used to implement proposed strategies*

DTC/PTC algorithms (DTC-II, DTC-III, PTC-II and PTC-III) provides similar dynamic performance of classical DTC/PTC strategy (DTC-I and PTC-I).

5.2 Experimental results

The proposed DTC/PTC strategies experimentally tested on dual inverter fed OEWIM drive. The experimental set-up used to implement proposed DTC/PTC strategies is shown in Fig. 13. The experimental studies are performed by implementing proposed algorithms with dSPACE DS-1104 controller board. The switching pulses from the controller are given to the inverters. The feedback signals required to implement the proposed algorithms are obtained by speed encoder, two voltage sensors: (LV-25) to measure DC-link voltage and two current sensors: (LA-25) to measure phase currents. The sampling time used to implement the proposed DTC and PTC strategies is 80 µs. OEWIM drive is coupled with separately excited DC generator; the load torque is applied by connecting resistive load bank to DC generator.

Figs. 14 and 15 shows experimental results of OEWIM drive for step changes in speed from forward motoring to reverse motoring. OEWIM drive is subjected to operate at 250 rad/s and −250 rad/s. Figs. 14 and 15 also represents the dynamic characteristics of proposed DTC and PTC strategies, the proposed algorithms provide high dynamic performance as similar to classical DTC/PTC. From Figs. 14*a* and 15*a*, it is observed that the torque ripples are less in PTC-I with respect to DTC-I. From Figs. 14*a* and *b*, the proposed DTC-II strategy gives lesser ripples in torque and flux when compared with DTC-I. The proposed DTC and PTC strategies provide lesser ripples in torque and flux with

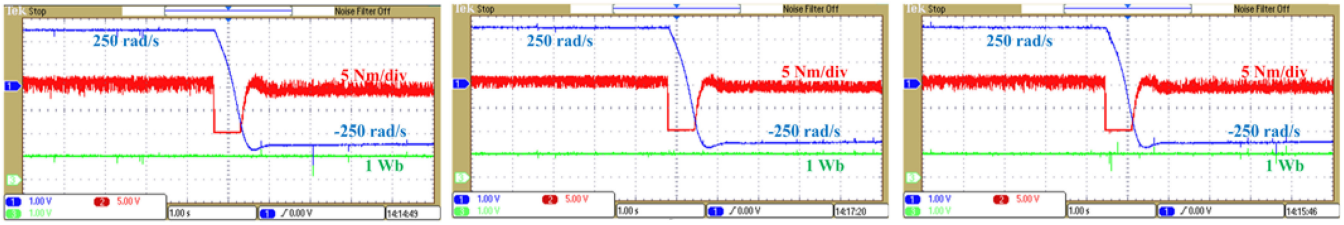

a b c

Fig. 14 *Experimental response of torque and flux of OEWIM drive for speed variation of 250 rad/s to −250 rad/s*
(a) DTC-I, ***(b)*** DTC-II and, ***(c)*** DTC-III

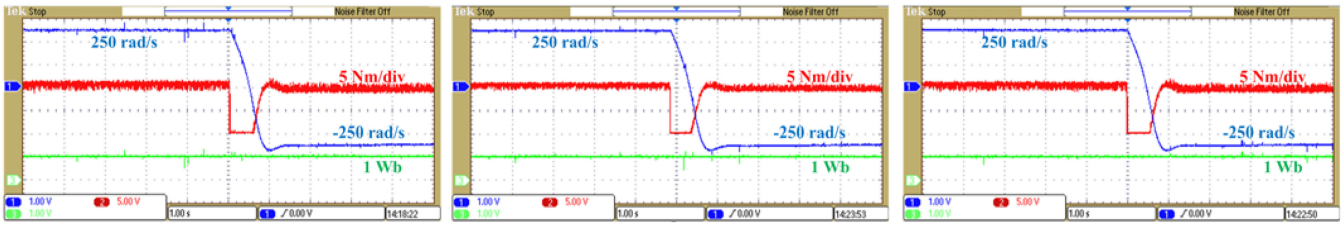

a b c

Fig. 15 *Experimental response of torque and flux of OEWIM drive for speed variation of 250 rad/s to −250 rad/s*
(a) PTC-I, ***(b)*** PTC-II and, ***(c)*** PTC-III

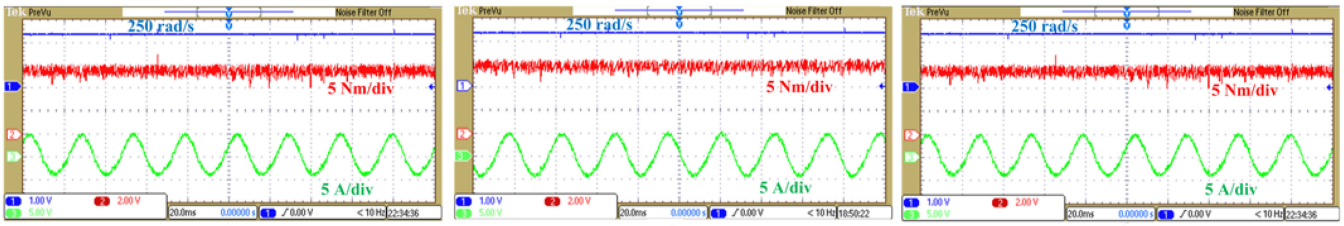

a b c

Fig. 16 *Speed, torque and current of OEWIM drive at a steady speed of 250 rad/s and a load torque of 14 Nm*
(a) DTC-I, ***(b)*** DTC-II and, ***(c)*** DTC-III

respect to classical DTC/PTC strategies and it is identified from Figs. 14 and 15.

Figs. 16 and 17 represents speed, torque, and current of OEWIM drive at a steady speed of 250 rad/s for DTC-I, DTC-II, DTC-III, PTC-I, PTC-II, and PTC-III. The currents are shown for the operation of OEWIM at a load torque of 14 Nm and speed of 250 rad/s ∼1193 rpm. The current THD (total harmonic distortion) of DTC-I, DTC-II and DTC-III at load torque of 14 Nm is 7.12, 5.24 and 6.68%. The current THD of PTC-I, PTC-II, and PTC-III are 4.48, 3.94 and 4.42%. From the THD of phase currents of OEWIM drive PTC-II gives lower distortions in current when compared with all other DTC/PTC strategies. The current distortions in PTC-I is lower than current distortions in DTC-I. The THD of PTC-III is slightly more than PTC-II but it is lower than PTC-I. Fig. 18 demonstrates voltage and CMV of OEWIM drive at a steady speed of 250 rad/s for DTC-I, DTC-II, and DTC-III. Fig. 19 demonstrates voltage and CMV of OEWIM drive at a steady speed of 250 rad/s for PTC-I, PTC-II, and PTC-III. The CMV is zero for DTC-III and PTC-III. From Figs. 18*c* and 19*c*, it is evident that the proposed DTC or PTC algorithms eliminate CMV. Fig. 20 represents switching transitions involved in PTC strategies of OEWIM drive at a steady speed of 250 rad/sec. From Fig. 20, the switching transitions involved in the implementation of PTC-III are less with respect to PTC-I and PTC-II. Table 8 represents performance analysis of OEWIM drive with classical DTC, Proposed DTC and recent DTC strategies. In [24], to reduce CMV only active voltage vectors are used because the use of null vector increases CMV. By neglecting null vector in DTC [24] torque ripple, flux ripple and distortions in current increase. DTC algorithm used in [32] utilises modified switching state tables for its operation; therefore, it gives less ripples in torque and flux when compared with DTC-I. Torque ripple and flux ripples are measured by taking sum of the difference between measured and reference values of torque and flux over 1,25,000 samples. The switching frequency is calculated by measuring the number of commutations of power devices from Table 9. Table 9 represents performance indices of OEWIM drive with classical PTC, proposed PTC and recent PTC strategies. In [34], modified cost function is used to reduce CMV and CMV term is included into the cost function; therefore, it increases number of weighting factors and needs more computations. Self-tuning of weighting factors is used in [36], it reduces the complex tuning of weighting factor but it needs more computations and increases torque, flux ripples. From Tables 8 and 9, it is observed that DTC-III and PTC-III gives less torque and flux ripples with zero CMV when compared with classical DTC and PTC strategies (DTC-I and PTC-I). DTC-II and PTC-II also gives lesser ripples in torque, flux and fewer distortions in current, these DTC and PTC strategies cannot eliminate CMV. In many of industrial applications, it is necessary to control number of commutations of high power switches, for those applications PTC-III is preferable. The proposed DTC/PTC strategies offer several benefits like zero CMV, reduced torque, flux ripples, and reduced switching frequency. The computational time required for developing the proposed DTC and PTC strategies are shown in Table 10. From Table 10, it is evident that the PTC strategies require more computational time than DTC strategies, whereas the performance of PTC strategies is better than DTC strategies. In summary, the limitations of classical DTC can circumvent by proposed PTC strategies. The proposed DTC and PTC strategies eliminate CMV, weighting factors, without losing features of classical DTC/PTC, and provide lesser ripple in torque, flux and less switching frequency.

6 Conclusion

In this article, enhanced DTC and PTC strategies implemented to an OEWIM drive with novel switching state algorithms. One of the limitation of DTC-I and PTC-I is higher CMV. The proposed DTC and PTC algorithms eliminate CMV by introducing selective voltage states to dual inverter fed OEWIM drive. The dual inverter

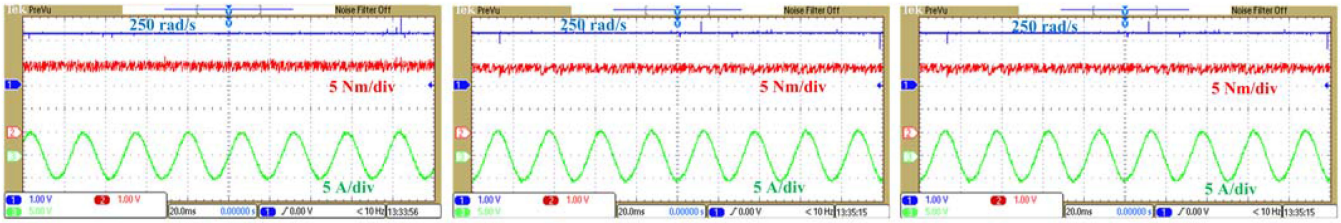

Fig. 17 *Speed, torque and current of OEWIM drive at a steady speed of 250 rad/s and a load torque of 14 Nm*
(a) PTC-I, ***(b)*** PTC-II and, ***(c)*** PTC-III

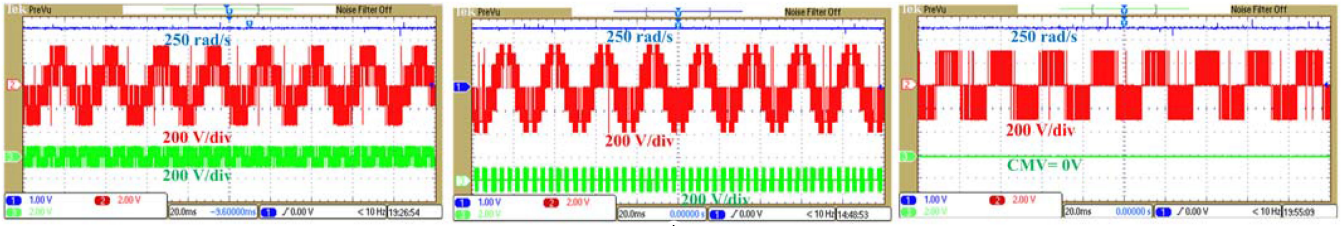

Fig. 18 *Experimental response of voltage and CMV at a speed of 250 rad/s*
(a) DTC-I, ***(b)*** DTC-II and, ***(c)*** DTC-III

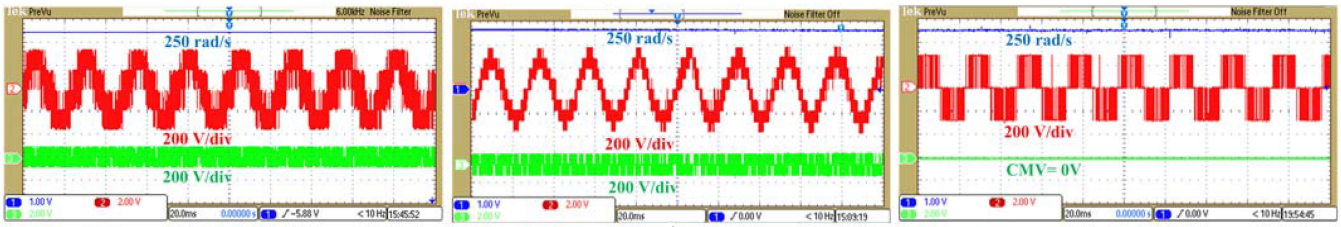

Fig. 19 *Experimental response of voltage and CMV at a speed of 250 rad/s*
(a) PTC-I, ***(b)*** PTC-II and, ***(c)*** PTC-III

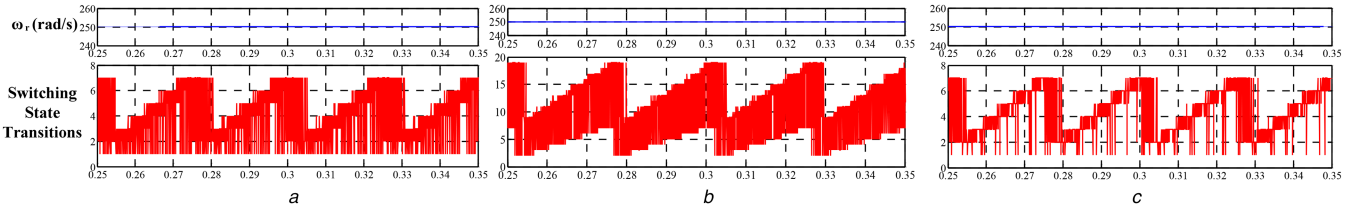

Fig. 20 *Voltage space vector transitions at a steady speed of 250 rad/s*
(a) PTC-I, ***(b)*** PTC-II and, ***(c)*** PTC-III

Table 8 Comparison of steady-state torque, flux ripple, switching frequency, CMV and Current THD of Proposed DTC Algorithms with Classical and Recent literature

	DTC-I			DTC-II			DTC-III			DTC [24]			DTC [32]		
Speed (rad/s)	100	200	250	100	200	250	100	200	250	100	200	250	100	200	250
torque ripple (Nm)	2.75	2.68	2.52	2.12	2.19	2.35	2.61	2.55	2.43	3.01	2.92	2.87	2.05	2.23	2.5
flux ripple (Wb)	0.057	0.048	0.045	0.039	0.036	0.032	0.052	0.046	0.042	0.062	0.056	0.054	0.048	0.042	0.036
CMV (V) (rms)	68	75	81	52	58	65	0	0	0	56.8	67.5	72	54.82	60.25	65.4
current THD (%)	6.41	6.92	7.12	4.35	4.86	5.24	6.12	6.43	6.68	5.69	7.14	7.51	4.62	5.18	5.32

Table 9 Comparison of steady-state torque, flux ripple, switching frequency, CMV and Current THD of Proposed PTC Algorithms with Classical and Recent literature

	PTC-I			PTC-II			PTC-III			PTC [34]			PTC [36]		
Speed (rad/s)	100	200	250	100	200	250	100	200	250	100	200	250	100	200	250
torque ripple (Nm)	2.5	2.25	2.15	1.68	1.42	1.35	2.14	1.93	1.65	1.88	1.69	1.48	1.94	1.83	1.74
flux ripple (Wb)	0.035	0.032	0.025	0.028	0.024	0.02	0.033	0.031	0.028	0.03	0.027	0.023	0.03	0.028	0.026
switching frequency (Hz)	4252	4527	4381	3895	4206	3928	3462	3971	3635	3785	4169	3845	3942	4128	3845
CMV (V) (rms)	58	67	77	49.5	56.8	62.3	0	0	0	53.8	58.6	66	56.9	62.5	68.2
current THD (%)	5.26	4.92	4.48	4.38	4.31	3.94	5.02	4.76	4.52	4.52	4.29	4.14	4.68	4.53	4.24

Table 10 Computational time needed to develop various DTC and PTC strategies

DTC Strategy	Computational time, μs	PTC strategy	Computational time, μs
DTC-I	45.62	PTC-I	58.45
DTC-II	54.95	PTC-II	65.42
DTC-III	45.35	PTC-III	60.58

configuration has 19 space vector locations. The proposed DTC-III and PTC-III strategies used in this article utilises only seven voltage space vector locations; hence, the proposed algorithms reduce computational burden on controller when compared with DTC-II and PTC-II. Another limitation involved in PTC-I is higher switching frequency. To reduce switching frequency involved in the implementation of PTC of OEWIM drive (PTC-I & PTC-II), PTC-III is introduced. PTC-III uses a modified cost function, to reduce switching frequency. DTC-II and PTC-II are developed by using all voltage space vectors of dual inverter configuration. DTC-II utilises a simplified look-up table and PTC-II eliminates the use of weighting factors into the cost function.

The effectiveness of proposed DTC and PTC strategies verified by conducting simulation and experimental studies on dual inverter fed OEWIM drive. From simulation and experimental results, PTC-III provides zero CMV, lesser torque ripple, flux ripple, and switching frequencies. Furthermore, the proposed DTC and PTC strategies offer all features of classical DTC and PTC (DTC-I and PTC-I), with simpler control algorithms. Finally, simplified DTC and PTC strategies have been developed to an OEWIM drive. The proposed DTC and PTC strategies provide lesser torque ripples, flux ripples, current distortions, zero CMV and weighting factor elimination.

7 Acknowledgments

This work was supported in part by the Science and Engineering Research Board (SERB)-Department of Science and Technology (DST) under grant no. SERB-DST/EEQ/2016/000188 and in part by the National Institute of Technology, Warangal.

8 References

[1] Takahashi, I., Noguchi, T.: 'A new quick-response and high-efficiency control strategy of an induction motor', *IEEE Trans. Ind. Appl.*, 1986, **IA-22**, (5), pp. 820–827

[2] Depenbrock, M.: 'Direct self-control (DSC) of inverter-fed induction machine', *IEEE Trans. Power Electron.*, 1988, **3**, (4), pp. 420–429

[3] Correa, P., Pacas, M., Rodriguez, J.: 'Predictive torque control for inverter-fed induction machines', *IEEE Trans. Ind. Electron.*, 2007, **54**, (2), pp. 1073–1079

[4] Zhong, L., Rahman, M.F., Hu, W.Y., *et al.*: 'Analysis of direct torque control in permanent magnet synchronous motor drives', *IEEE Trans. Power Electron.*, 1997, **12**, (3), pp. 528–536

[5] Buja, G.S., Kazmierkowski, M.P.: 'Direct torque control of PWM inverter-fed AC motors - a survey', *IEEE Trans. Ind. Electron.*, 2004, **51**, (4), pp. 744–757

[6] Abu-Rub, H., Iqbal, A., Guzinski, J.: '*High performance control of AC drives with matlab/simulink models*' (John Wiley & Sons, Inc., New York, 2012)

[7] Ogasawara, S., Ayano, H., Akagi, H.: 'Measurement and reduction of EMI radiated by a PWM inverter-fed AC motor drive system', *IEEE Trans. Ind. Appl.*, 1997, **33**, (4), pp. 1019–1026

[8] ABB Drives.: 'Bearing currents in modern AC drive systems', Technical Guide No. 5. ABB, 2011

[9] Cacciato, M., Consoli, A., Scarcella, G., *et al.*: 'Reduction of common-mode currents in PWM inverter motor drives', *IEEE Trans. Ind. Appl.*, 1999, **35**, (2), pp. 469–476

[10] Zhang, H., Von Jouanne, A., Dai, S., *et al.*: 'Multilevel inverter modulation schemes to eliminate common-mode voltages', *IEEE Trans. Ind. Appl.*, 2000, **36**, (6), pp. 1645–1653

[11] Akagi, H., Hasegawa, H., Doumoto, T.: 'Design and performance of a passive EMI filter for use with a voltage-source PWM inverter having sinusoidal output voltage and zero common-mode voltage', *IEEE Trans. Power Electron.*, 2004, **19**, (4), pp. 1069–1076

[12] Jain, S., Ramulu, C., Padmanadhan, S., *et al.*: 'Dual MPPT algorithm for dual PV source fed open-end winding induction motor drive for pumping application', *Eng. Sci. Technol., Int. J.*, 2016, **19**, (4), pp. 1771–1780

[13] Dehghani kiadehi, A., El Khamlichi Drissi, K., Pasquier, C.: 'Angular modulation of dual-inverter fed open-end motor for electrical vehicle applications', *IEEE Trans. Power Electron.*, 2016, **31**, (4), pp. 2980–2990

[14] Lu, S, Corzine, K.: 'Multilevel multi-phase propulsion drives'. IEEE Electric Ship Technologies Symp., 2005., Philadelphia, PA, 2005, pp. 363–370

[15] Lakhimsetty, S., Surulivel, N., Somasekhar, V.T.: 'Improvised SVPWM strategies for an enhanced performance for a four-level open-end winding induction motor drive', *IEEE Trans. Ind. Electron.*, 2017, **64**, (4), pp. 2750–2759

[16] Kunisetti, V.P.K., Kodumur Meesala, R.E., Thippiripati, V.K.: 'Improvised predictive torque control strategy for an open end winding induction motor drive fed with four-level inversion using normalised weighted sum model', *IET Power Electron.*, 2018, **11**, (5), pp. 808–816

[17] Miranda, H., Cortes, P., Yuz, J.I., *et al.*: 'Predictive torque control of induction machines based on state-space models', *IEEE Trans. Ind. Electron.*, 2009, **56**, (6), pp. 1916–1924

[18] Vinay Kumar, T., Rao, S.S.: 'Direct torque controlled induction motor drive based on cascaded three two-level inverters', *Int. J. Model. Simul.*, 2014, **34**, (2), pp. 70–82

[19] Habibullah, M., Lu, D.D.C., Xiao, D., *et al.*: 'A simplified finite-state predictive direct torque control for induction motor drive', *IEEE Trans. Ind. Electron.*, 2016, **63**, (6), pp. 3964–3975

[20] Zhang, Y., Yang, H.: 'Two-vector-based model predictive torque control without weighting factors for induction motor drives', *IEEE Trans. Power Electron.*, 2016, **31**, (2), pp. 1381–1390

[21] Karamanakos, P., Stolze, P., Kennel, R.M., *et al.*: 'Variable switching point predictive torque control of induction machines', *IEEE J. Emerg. Sel. Top. Power Electron.*, 2014, **2**, (2), pp. 285–295

[22] Zhang, Y., Yang, H.: 'Model predictive torque control of induction motor drives with optimal duty cycle control', *IEEE Trans. Power Electron.*, 2014, **29**, (12), pp. 6593–6603

[23] Saribulut, L., Teke, A., Tümay, M.: 'Vector-based reference location estimating for space vector modulation technique', *Electr. Power Syst. Res.*, 2012, **86**, pp. 51–60

[24] Cirrincione, M., Pucci, M., Vitale, G., *et al.*: 'A new direct torque control strategy for the minimization of common-mode emissions', *IEEE Trans. Ind. Appl.*, 2006, **42**, (2), pp. 504–517

[25] Renge, M.M., Suryawanshi, H.M.: 'Three-dimensional space-vector modulation to reduce common-mode voltage for multilevel inverter', *IEEE Trans. Ind. Electron.*, 2010, **57**, (7), pp. 2324–2331

[26] Kalaiselvi, J., Srinivas, S.: 'Bearing currents and shaft voltage reduction in dual-inverter-fed open-end winding induction motor with reduced CMV PWM methods', *IEEE Trans. Ind. Electron.*, 2015, **62**, (1), pp. 144–152

[27] Kumar, P.R., Rajeevan, P.P., Mathew, K., *et al.*: 'A three-level common-mode voltage eliminated inverter with single DC supply using flying capacitor inverter and cascaded H-bridge', *IEEE Trans. Power Electron.*, 2014, **29**, (3), pp. 1402–1409

[28] Behera, R.K., Das, S.P., Ojo, O.: 'Analysis and experimental investigation of CM voltage mitigation of a high performance induction motor drive'. 2012 IEEE Int. Conf. on Power Electronics, Drives and Energy Systems (PEDES), Bengaluru, 2012, pp. 1–6

[29] Kumar, K.V.P., Kumar, T.V.: 'Experimental implementation of direct torque control of open end winding induction motor'. 2016 IEEE Region 10 Conf. (TENCON), Singapore, 2016, pp. 3318–3323

[30] Kumar, A., Fernandes, B.G., Chatterjee, K.: 'DTC of open-end winding induction motor drive using space vector modulation with reduced switching frequency'. 2004 IEEE 35th Annual Power Electronics Specialists Conf. (IEEE Cat. No.04CH37551), 2004, Vol. 2, pp. 1214–1219

[31] Vinod, B.R., Baiju, M.R., Shiny, G.: 'Five level inverter fed space vector based direct torque control of open-end winding induction motor drive', *IEEE Trans. Energy Convers.*, 2018, **33**, (3), pp. 1392–1401, doi: 10.1109/TEC.2018.2824350

[32] Praveen Kumar, K.V., Vinay Kumar, T.: 'An effective four-level voltage switching state algorithm for direct torque controlled open end winding induction motor drive by using two two-level inverters', *Electr. Power Compon. Syst.*, 2018, **45**, (19), pp. 2175–2187

[33] Praveen Kumar, K.V., Vinay Kumar, T.: 'An enhanced three-level voltage switching state scheme for direct torque controlled open end winding induction motor', *J. Inst. Eng. India- Series B*, 2018, **99**, (3), pp. 235–243, doi: 10.1007/s40031-017-0311-7 (in early access)

[34] Praveen Kumar, K.V., Vinay Kumar, T.: 'Predictive torque control of open-end winding induction motor drive fed with multi-level inversion using two two-level inverters', *IET-Electr. Power Appl.*, 2018, **12**, (1), pp. 54–62

[35] Meesala, R.E.K., Kunisetti, V.P.K., Thippiripati, V.K.: 'Enhanced predictive torque control for open end winding induction motor drive without weighting factor assignment', *IEEE Trans. Power Electron.*, 2019, **34**, (1), pp. 503–513, doi: 10.1109/TPEL.2018.2812760 (in early access)

[36] Praveen Kumar, K.V., Ravi Eswar, K.M., Vinay Kumar, T.: 'Hardware implementation of predictive torque controlled open end winding induction motor drive with self-tuning algorithm', *Cogent Eng.*, 2017, **4**, (1), pp. 1–17

[37] Zhu, B., Rajashekara, K., Kubo, H.: 'Comparison between current-based and flux/torque-based model predictive control methods for open-end winding induction motor drives', *IET Electr. Power Appl.*, 2017, **11**, (8), pp. 1397–1406

[38] Kalantari, N., Lopes, L.A.C.: 'Reduction of dead-time effect on the common mode voltage of an open-end winding machine'. 2016 IEEE 25th Int. Symp. on Industrial Electronics (ISIE), Santa Clara, CA, 2016, pp. 836–841

[39] Vas, P.: '*Sensorless vector and direct torque control*' (Oxford University Press, New York, 1998)